CHAPTER - IV

ASSESSMENT OF SEAWATER ELECTROLYSIS ON PLATNIZED TIN AND MAGNESIUM ALLOY NANOPARTICLES FOR NON-MEMBRANE POWER SYSTEMS

4.1 INTRODUCTION

The choice of seawater electrolyte is superior to facilitate the fuel cell development, make as the practice more efficient for fuel cell technologies. Seawater as electrolyte for non-membrane ethanol fuel cell (MLEFC) enhances the hydrogen production during the electrochemical reaction. The use of ethanol as a fuel in membraneless ethanol fuel cell (MLEFC) has several advantages compared to that of hydrogen such as transport and storage, ease of handling and low operating temperature, and a high energy density (Ren et al, 2000; Choi et al, 2004; Yamaguchi et al, 2005).

Platinum was initially used as an electrocatalyst in the anode, as it was known to be the best electrocatalyst for the electro-oxidation of ethanol. However, the use of platinum is limited due to the CO poisoning effect; therefore, the use of binary electrocatalysts, where a new metal is added onto the Pt-base, has been studied (Xu et al, 2006; Luo et al, 2006; Shobha et al, 2003).

It is well known that the addition of Ru to Pt-based electrocatalysts lowers the over potential for the ethanol electro-oxidation reaction via the so-called bifunctional mechanism (Gasteiger et al, 1993; Markovic et al, 1995; Yajima et al, 2004). Wang et al, (2009) suggesting that tin and tungsten atoms either form an alloy with platinum or exist as amorphous oxide phases. Due to the strong adsorption of CO onto the Pt

surface, the hydrogen adsorption-desorption of the Pt was completely blocked in the hydrogen region indicating the presence of a saturated CO adlayer (Choi et al, 2003). In non-membrane fuel cells, pure Pt/C catalyst does not behave as a very good anode for ethanol electro-oxidation due to its poisoning by strongly adsorbed intermediates such as CO and CH_3COOH (Vigier et al, 2004).

To further increase the catalytic activity of the anode, the introduction of a third metal to Pt–Sn/C binary catalyst was found to be the best electrocatalyst, because of its higher tolerance to CO poisoning. Therefore, new alternative materials for electrocatalysts are required to minimize the noble metal loading and to optimize the catalytic performance.

In this regard, many authors have intensively investigated Pt-based binary and ternary compounds to improve the performance of the electrocatalysts for the electrooxidation of ethanol (Sivakumar et al, 2006; Neto et al, 2007; Wang et al, 2009; Kang et al, 2010; Chen et al, 2014). Hence, we prepared Pt–Sn–Mg/VC ternary alloy electrocatalysts by using thermal reduction method.

Gowdhamamoorthi et al, (2014) and Ponmani et al, (2014) also demonstrated that the performance of the developed non-membrane fuel cell enhanced profoundly if the concentration of oxidant in cathodic stream is 10 times larger, and the current density is also increased approximately ten times.

The enhanced activity of the ternary catalyst is due to the promoting effect of the second or third elements added to Pt. In the present study, we evaluated the catalytic activity for ethanol oxidation reaction (EOR) by incorporating Mg to Pt–Sn/VC catalysts in MLEFC.

4.2 EXPERIMENTAL

4.2.1 Materials

The metal precursors used for the preparation of electrocatalysts were $H_2PtCl_6.6H_2O$ (from Sigma Aldrich), $SnCl_2.3H_2O$ (from Sigma Aldrich) and $MgSO_4.7H_2O$ (from Sigma Aldrich). Vulcan XC-72R carbon black (from Cabot Corp.,) was used as a support for the catalysts. Graphite plates (from E-TEK) were used as substrates for the catalyst to prepare the electrodes. Nafion® (DE 521, DuPont USA) dispersion was used to make the catalyst slurry. Isopropyl alcohol (from Merck) was used as a solvent and $NaBH_4$ (from Merck) was used as the reduction agent. Ethanol (from Merck), sodium perborate (from Riedel) and H_2SO_4 (from Merck) and seawater were used as the fuel, the oxidant and as the electrolyte for electrochemical analysis, respectively. All the chemicals were of analytical grade. Pt/VC (40-wt%, from E-TEK) was used as the cathode catalyst.

4.2.2 Catalyst Preparation

Vulcan carbon supported ternary Pt–Sn–Mg catalysts with different atomic ratios were synthesized by thermal reduction method (Wang et al, 2009). The carbon black was ultrasonically dispersed in a mixture of ultrapure water (Millipore MilliQ, 18 MΩ cm), and isopropyl alcohol for 20 min. Then the precursors were added to the ink, and then mixed thoroughly for 20 min. The ink was dried with a magnetic stirrer at 60 ◦C. The dried $H_2PtCl_6.6H_2O$, $SnCl_2.3H_2O$ and $MgSO_4.7H_2O$ compounds with carbon were put into a tube furnace and reduced at 400 °C with a gaseous mixture of H_2 and Ar with an atomic ratio of 1:9. The catalyst powder was stored in a vacuum vessel. For comparison, the monometallic Pt/VC, bimetallic Pt–Sn/VC and Pt–Mg/VC catalysts

were synthesized under the same conditions. The electrocatalytic mixtures and atomic ratios were $Pt_{50}Sn_{40}Mg_{10}$/VC, $Pt_{50}Sn_{30}Mg_{20}$/VC, $Pt_{50}Sn_{25}Mg_{25}$/VC, $Pt_{50}Sn_{50}$/VC, $Pt_{50}Mg_{50}$/VC and Pt_{100}/VC. The nominal loading of metals in the electrocatalysts was 40 %wt and rest 60 %wt was carbon.

4.2.3 Physical Characterization

The morphology of the dispersed catalysts was examined using TEM (Philips CM 12 Transmission Electron Microscope). The particle size distribution and mean particle size were also evaluated using TEM. The crystal structure of the synthesized electrocatalysts was characterized by powder X-ray diffraction (XRD) using a Rigaku multiflex diffractometer (model RU-200 B) with Cu-$K_{\alpha 1}$ radiation source ($\lambda_{K\alpha 1}$ = 1.5406 A^o) operating at room temperature. The tube current was 40 mA with a tube voltage of 40 kV. The 2θ angular regions between 20º and 90º were recorded at a scan rate of 5° min^{-1}. The mean particle size analyzed from TEM is verified by determining the crystallite size from XRD pattern using Scherrer formula. Pt (2 2 0) diffraction peak was selected to calculate crystallite size and lattice parameter of platinum. According to Scherrer's equation (Radmilovic et al, 1995)

$$d = \frac{0.9\lambda_{K\alpha 1}}{ß_{2\theta} \cos \theta_{max}} \qquad (4.1)$$

Where d is the average crystallite size, θ_{max} is the angle at the position of the peak maximum, $ß_{2\theta}$ is the width of the peak (in radians), 0.9 is the shape factor for spherical crystallite and $\lambda_{K\alpha 1}$ is the wavelength of X-rays used. The lattice parameters of the catalysts were estimated according to equation 4.2 (Radmilovic et al, 1995)

$$a = \frac{\sqrt{2}\,\lambda_{K\alpha 1}}{\text{Sin}\,\theta_{max}} \qquad (4.2)$$

where a, is the lattice parameter (nm) and all the other symbols have the same meanings as in equation 4.1 (Beyan et al, 2013). The atomic ratio of the catalysts was determined by an energy dispersive X-ray (EDX) analyzer, which was integrated with the TEM instrument.

4.2.4 Electrochemical Measurement

Electrochemical studies of the electrocatalysts were carried out using the thin porous coating technique (Colmati et al, (2007). All electrochemical measurements were performed on an electrochemical workstation (CH Instruments, model CHI6650, USA) interfaced with a personal computer using the CHI software, at room temperature. A common three-electrode electrochemical cell using cyclic voltammetry (CV) and chronoamperometry (CA) techniques was used for the measurements. Catalyst coated glassy carbon electrode (GCE, 3 mm diameter and 0.071 cm^2 of electrode area, from CHI, USA) was used as the working electrode and platinum foil was used as the counter electrode.

Ag/AgCl in saturated KCl was used as the reference electrode (RHE). The working electrode was prepared by applying catalyst ink made of 20 mg of electrocatalyst in a solution of 50 mL of water containing three drops of 6% PTFE suspension. The resulting mixture was treated in an ultrasound bath for 10 min to obtain a uniform dispersion. The catalyst slurry was then drop-cast on to a glassy carbon electrode and allowed to dry at 100 ºC for 30 min.

For assessing the electrocatalytic activity of the working electrode, cyclic voltammetry was obtained in 1.0 M ethanol and 0.5 M H_2SO_4 solution with a scan rate of 50 mV s^{-1}. The electrochemically active surface areas (SEAS) of the electrocatalyts were calculated by using Eq. (4.1) (Zhou et al, 2003; Bonesi et al, 2010; Beyhan et al, 2013). The onset potential for the oxidation of ethanol in a positive scan was a key factor for evaluating the catalyst activity (Cao et al, 2007). For the durability test, the chronoamperometric experiments were carried out at 0.1 V for 2500 s in the same electrolyte. Before each measurement, the solution was purged with high-purity nitrogen gas for at least 30 min to ensure oxygen-free measurements.

4.2.5 Single Cell Test

In the present study, we fabricated the non-membrane ethanol fuel cell (MLEFC) using laminar flow-based fuel cell configuration (Arun et al, 2014; Ponmani et al, 2014). In this non-membrane fuel cell, ethanol is used as a fuel, sodium perborate is used as an oxidant and seawater is used as an electrolyte. In non-membrane fuel cell system seawater used as electrolyte for more accurate that allows both high energy density and low environmental impact at a low cost. In crystalline state sodium perborate exist as a dimeric peroxo-salt with water of hydration, but in aqueous solution affords hydrogen peroxide (Cotton et al, 1988) as shown in Eq. (4.3),

$$[B(OH)_3(O_2H)]^- + H_2O \rightleftharpoons [B(OH)_4]^- + H_2O_2 \qquad (4.3)$$

In MLEFC, the aqueous fuel and oxidant streams flow in parallel in a single microchannel with the anode and cathode on opposing sidewalls (**Fig. 4.1**). Graphite plates of one mm thickness served as current collectors and catalyst support structures. The different anode and cathode catalysts were coated onto the graphite plates. For

single cell, the anode catalysts with different atomic ratios were prepared as follows: The catalyst ink was prepared by mixing required quantity of catalyst with a solution of 50 mL of water containing three drops of 6% PTFE dispersion in an ultrasonic bath for 10 min to obtain a uniform dispersion. The catalyst slurry was then spread on the graphite plate by brush and dried at 100 ºC for 30 min to obtain anode and cathode electrodes. The catalysts tested on the anode side were $Pt_{50}Sn_{40}Mg_{10}$/VC, $Pt_{50}Sn_{30}Mg_{20}$/VC, $Pt_{50}Sn_{25}Mg_{25}$/VC, $Pt_{50}Sn_{50}$/VC, $Pt_{50}Mg_{50}$/VC and Pt_{100}/VC, Pt with catalyst loading 2 mg/cm^2. On the cathode side, Pt/VC (100) with catalyst loading 2 mg/cm^2 was used in all experiments. The two catalyst-coated graphite plates were aligned to form a channel with 0.1 cm electrode-to-electrode distance (width), a 3 cm length, and a 0.1 cm height. The anolyte (fuel and electrolyte) and catholyte (oxidant and seawater) streams flow in a laminar fashion over the anode and cathode, respectively.

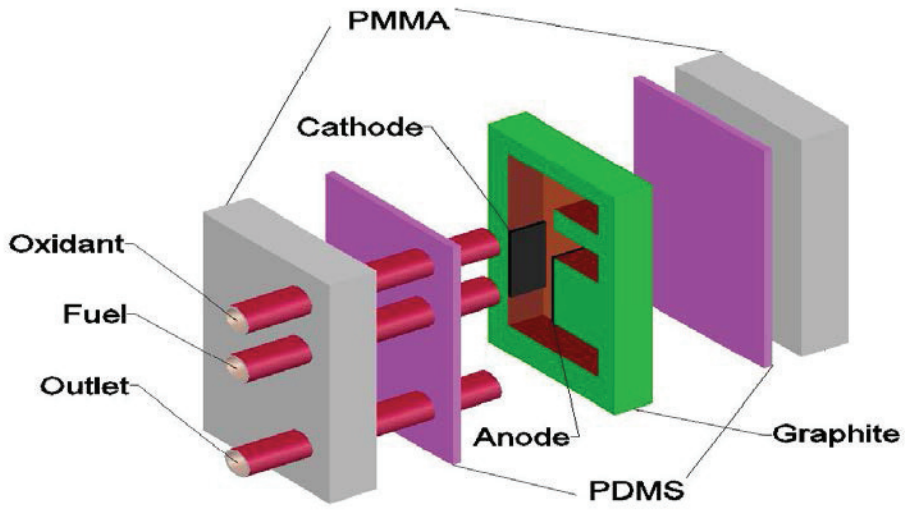

Fig. 4.1 Schematic of the E-shaped membraneless laminar flow based fuel cell with graphite plates molded with poly(dimethylsiloxane) and sealed with poly(methylmethacrylate).

The electrode area along a microchannel wall between the inlets and the outlet (3 cm long and 0.1 cm wide) was used as the geometric surface area of the electrodes in this study (0.3 cm^2). The design is described in detail elsewhere (Choban et al, 2004; Jayashree et al., 2010). The anolyte used in the anode side was 1.0 M ethanol + 0.5 M H_2SO_4 and the catholyte used in the cathode side was 0.1 M perborate in seawater. The flow rate of each of the streams was 0.3 mL min^{-1} (total flow rate of 0.6 mL min^{-1}). The MLEFC was operated at room temperature. The current-voltage characteristics of MLEFC were measured using an electrochemical workstation (CH Instruments, model CHI6650, USA) and the data was verified using a multi-meter (MASTECH® MAS830L).

4.3 RESULTS AND DISCUSSIONS

4.3.1 Analysis of Physical Significance

4.3.1.1 XRD – X-Ray Diffraction

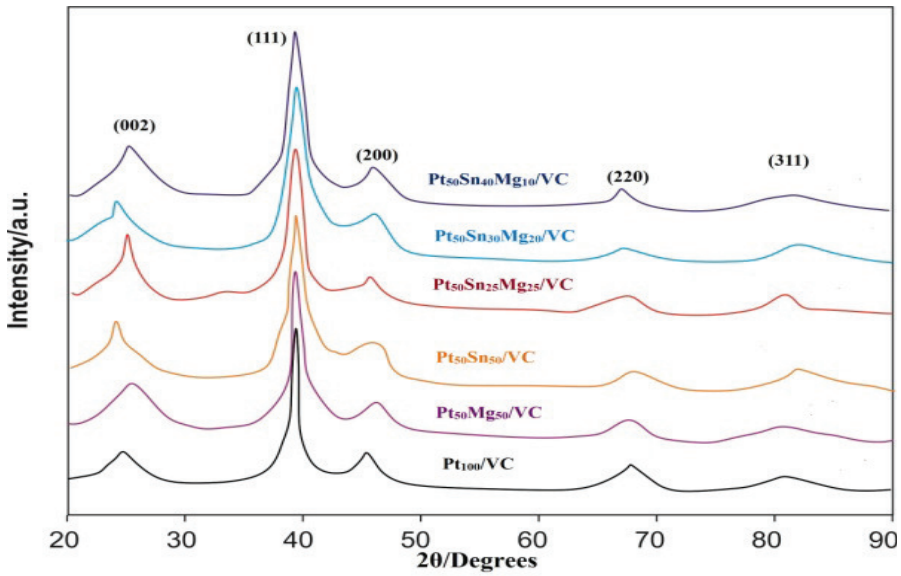

Fig. 4.2 X-ray diffraction peaks of Pt−Sn−Mg (50:40:10), Pt−Sn−Mg (50:30:20), Pt−Sn−Mg (50:25:25), Pt−Mg (50:50), Pt−Sn (50:50) and Pt (100) nanoparticles.

XRD analysis was used to establish the atomic structure of the prepared crystalline catalysts. **Fig. 4.2** shows the XRD peaks of Vulcan carbon-support (VC) assisted Pt−Sn−Mg (50:40:10), Pt−Sn−Mg (50:30:20), Pt−Sn−Mg (50:25:25), Pt−Mg (50:50), Pt−Sn (50:50) and Pt (100) nanoparticles. For all the synthesized catalysts, the wide peak obtained between 25° and 30° is affiliated with the zero-zero-two plane of the six-membered hexagon architecture for carbonaceous supports. Together with, peaks of 2θ appearing at 38.8°, 47.7°, 68.8° and 81.6° are analogous of significant planes of 111, 200, 220, and 311 relevant to the unique face-centered-cubic (FCC) nature of metallic platinum.

The XRD patterns of the prepared catalysts showed that all the diffraction peaks were apparently shifted to higher 2θ values with respect to the corresponding peaks of the platinum catalyst, indicating an interlace augmentation arising from the incorporation of the second and the third atoms into the Pt lattice due to the formation of VC-support assisted Pt–Sn–Mg alloy nanoparticles.

The XRD patterns of Pt–Sn–Mg/VC nanoparticles do not illustrate any peaks of magnesium or magnesium oxides. Despite their characteristic appearance cannot be ruled out, because the magnesium particles probably exist in smaller size or present in an amorphous form.

The Scherrer's formula is used to calculate the average particle size of the Pt/VC, Pt−Sn/VC, Pt−Mg/VC, Pt−Sn−Mg/VC (50:25:25), Pt−Sn−Mg/VC (50:30:20) and Pt−Sn−Mg/VC (50:40:10), alloyed-nanoparticles prepared with the platinum content. The average size of Pt-Mg/VC, Pt-Sn/VC as well as Pt-Sn-Mg/VC nanoparticles is smaller than that of the Pt/VC prepared with the similar procedure

shown in **Table 4.1.** The reduction in lattice parameters reveals the inclusion of a second (Sn) and a third metal (Mg) into Pt. The average elemental-size regarding Pt/Sn/Mg nanoparticles on VC support were in the range of 3.0 to 4.0 nanometers.

Table 4.1 The composition and particle size of synthesized nanoparticles.

Alloy Nanoparticles	Initial atomic ratio (nm)			Estimated atomic ratio (nm)			Structural lattice-periodicities (nm)	Mean crystallite size (nm)	TEM Particle size (nm)
	Pt	Sn	Mg	Pt	Sn	Mg			
Pt/VC	100	–	–	97	–	–	0.3914	4.3	4.0
Pt-Mg/Vc	50	–	50	52	–	48	0.3898	4.1	3.9
Pt-Sn/VC	50	50	–	51	49	–	0.3905	3.6	3.5
Pt-Sn-Mg/VC	50	25	25	51	25	24	0.3903	3.5	3.2
Pt-Sn-Mg/VC	50	30	20	51	28	21	0.3897	3.4	3.2
Pt-Sn-Mg/VC	50	40	10	52	38	10	0.3894	3.2	3.0

4.3.1.2 TEM–Transmission Electron Microscopy

TEM-Transmission electron microscopy analyses be executed in order to investigate the particle sizes concerning Vulcan carbon-support assisted Pt−Sn−Mg nanoparticles. **Fig. 4.3** shows the prototypical transmission electron microscopy illustrations of the synthesized platinum alloy nanoparticles. TEM images reveal that the metal particles are nanosized and evenly transfused on VC. Further, TEM images

clearly show that each individual catalysts are spherical in shape and having the size of below five nanometers with slight agglomeration. The reason for agglomeration is due to the rapid reduction process of the catalysts. As a matter of fact, the dissemination of the synthesized nanoparticles are confined towards systematically for certain range. Consequently, the dispersion of nanoparticles on TEM analysis was carried out by wildly choosing proportionate number of particles related to each TEM illustrations. Correspondingly, the size of nanoparticles obtained is between three and four nanometers, with 3.0 -3.2 nm for Pt−Sn−Mg/VC, nanoparticles. Moreover, the TEM illustrations witnessed that the proportions of Pt−Sn−Mg/VC nanoparticles were lesser than that of the binary Pt−Sn/VC as well as Pt−Mg/VC nanoparticles.

Table 4.1 summarizes the results of TEM analysis towards the particle size dissemination and histogram analysis of synthesized nanoparticles.

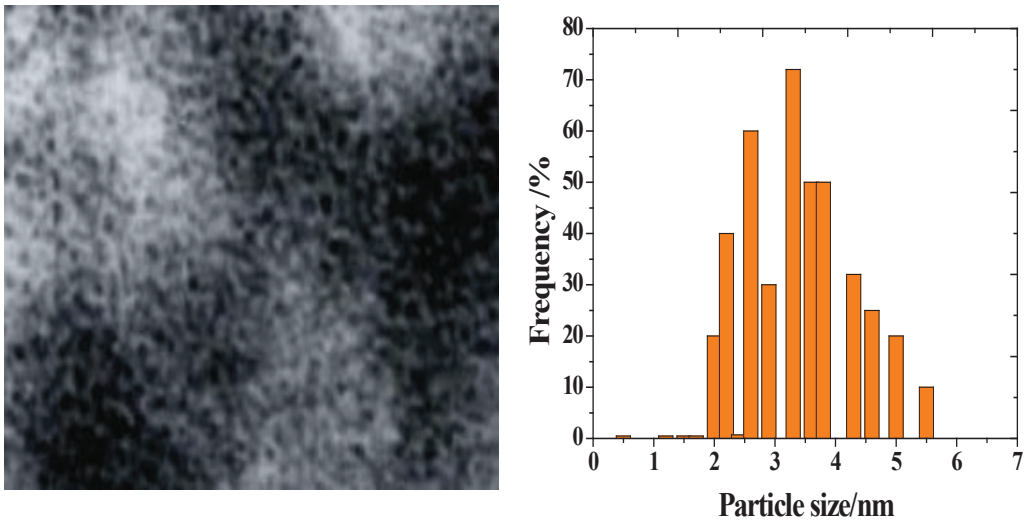

Fig. 4.3 Micrographs of transmission electron microscopy and its histograms of Pt/Sn/Mg alloyed nanoparticles on VC support.

At the same time, the overall particle-proportions established through TEM illustrations and x-ray diffraction investigations were coincidental with each other. Also, the particle size of Vulcan carbon-support assisted Pt−Sn (50:50) was analogous to that of Pt−Mg/VC (50:50) nanoparticles.

4.3.1.3 EDX – Energy Dispersive X-ray Microanalysis

EDX is a powerful method to characterize the chemical composition and texture concerning Pt−Sn−Mg nanoparticles supported on Vulcan carbon. The EDX spectra shown in **Fig. 4.4** inveterate the presence of Pt, Sn, Mg nanoparticles along with amorphous carbon. In essence, the EDX results are exhibited in **Table 4.1**. A minimum variation of the atomic ratio is observed in the prepared catalysts with the desired elements.

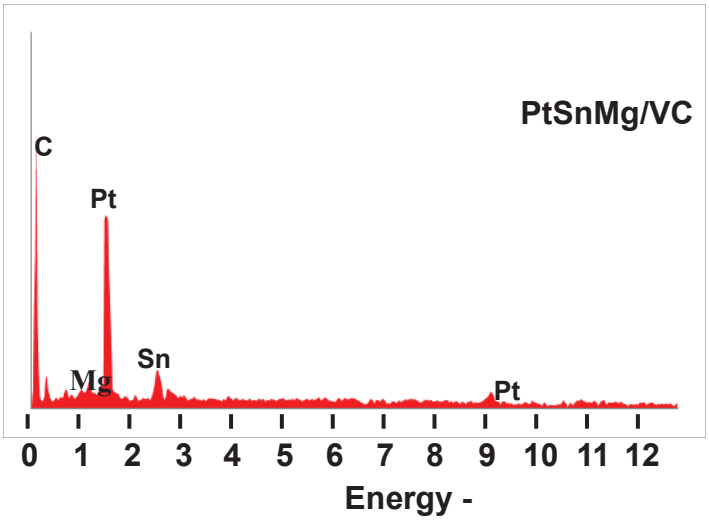

Fig. 4.4 Microanalysis spectrum of EDX for Pt/Sn/Mg nanoparticles on VC support.

As a consequence, the EDX spectra shown in Fig. 4.4 reflected the presence of Pt, Sn, and Mg nanoparticles along with the amorphous carbon. As can be seen, a minimum variation of an atomic ratio is observed in the prepared nanoparticles with the

expected elements. Meanwhile, the actual metallic ratio of the synthesized catalyst consent well with the nominal value.

4.3.2 Analysis of Electrochemical Significance

4.3.2.1 CV – Cyclic voltammetry

In this study, cyclic voltammetry is used to characterize the electrode mechanism involved in the nanoparticles synthesized by thermal reduction method. **Fig. 4.5(a)** represents the cyclic voltammograms of the $Pt_{50}Sn_{40}Mg_{10}$/VC, $Pt_{50}Sn_{30}Mg_{20}$/VC, $Pt_{50}Sn_{25}Mg_{25}$/VC, $Pt_{50}Sn_{50}$/VC, $Pt_{50}Mg_{50}$/VC, and Pt_{100}/VC alloyed nanoparticles disbursed onto the glassy carbon electrode in the absence of fuel. It can be observed from the Fig. 4.5(a), the hydrogen adsorption and desorption on the active surface of platinum was severely affected by the formation of carbonaceous intermediates.

However, the current for all the bimetallic and trimetallic catalysts in the dual laminar range (from 40 to 80 mV versus RHE) is more related to monometallic platinum. In the final analysis, voltammograms activity of all the prepared nanoparticles shows a congruent characteristic of bifold and trifold platinum alloy catalysts incorporating transition elements.

Subsequently, the out-put values are adjusted into gram per mole of platinum, assuming that alcohol oxidation- reduction reaction appears exclusively onto the reactive sites of platinum at normal temperature. The electrochemical active surface area (S_{EAS}) for the Pt/Sn/Mg nanoparticles on VC support was estimated by using the following formula (4.4):

$$S_{EAS/CO}(m^2/g) = \frac{Q_{CO}(\mu C/cm^2)}{420(\mu C/cm^2) \times [Pt]} \quad (4.4)$$

where Q_{CO} is the CO charge on the catalyst surface, 420($\mu C/cm^2$) represents the current needed to oxidize CO intermediates. The non-smoothness of nanoparticles is determined by dividing the surface area with the available area. The estimated values are given in **Table 4.2**.

The real surface area estimated by this method is in good agreement with the enhancement in electrocatalytic activity. It is shown that Mg-modified Pt–Sn/VC surfaces offer energetically different sites for adsorption and oxidative desorption, which can be selectively populated by CO species either *via* the direct adsorption of CO dissolved in the electrolyte or *via* the adsorption and decomposition reaction of alcohol.

In conclusion, the topmost electrochemical area is accomplished by the trimetallic catalysts on VC support, owing to the structural modification of Pt/Sn by Mg. Appropriately, the functionality of trimetallic nanoparticles has been enhanced in terms of CO oxidation.

By comparing the Pt_{100}/VC as a reference, the electrocatalytic activity of binary $Pt_{50}Sn_{50}$/VC and $Pt_{50}Mg_{50}$/VC nanoparticles performed analogously to raw platinum particles. At the same time, a remarkable hike in the output voltage of ternary $Pt_{50}Sn_{40}Mg_{10}$/VC nanoparticle was noticed in the dual-layer region of 40mV to 80 mV, suggesting that the incorporation of third metal into binary Pt/Sn alloy is the reason for the enhancement of electro-kinetics towards alcohol oxidation. **Fig 4.5(b)** represents the cyclic voltammograms of $Pt_{50}Sn_{40}Mg_{10}$/VC, $Pt_{50}Sn_{30}Mg_{20}$/VC, $Pt_{50}Sn_{25}Mg_{25}$/VC, $Pt_{50}Sn_{50}$/VC, $Pt_{50}Mg_{50}$/VC and Pt_{100}/VC nanoparticles for alcohol oxidation in an acidic

medium. The initial commencement of achievable voltage is an important aspect of the assessment catalytic activity towards electro-oxidation of alcohol.

Table 4.2 Surface area periodicities of Pt/Sn/Mg alloy nanoparticles on VC support.

Nanopaticles	Q_{CO}/μC	Electrode real surface area (cm^2)	$S_{EAS/CO}$ (m^2/g_{Pt})[a]	Roughness
Pt_{100}/VC	1260	3.1	31	83.0
$Pt_{50}Mg_{50}$/VC	672	1.5	33	43.8
$Pt_{50}Sn_{50}$/VC	36	1.8	36	48.1
$Pt_{50}Sn_{25}Mg_{25}$/VC	841	2.0	41	56.4
$Pt_{50}Sn_{30}Mg_{20}$/VC	965	2.4	47	64.6
$Pt_{50}Sn_{40}Mg_{10}$/VC	1025	2.5	48	68.8

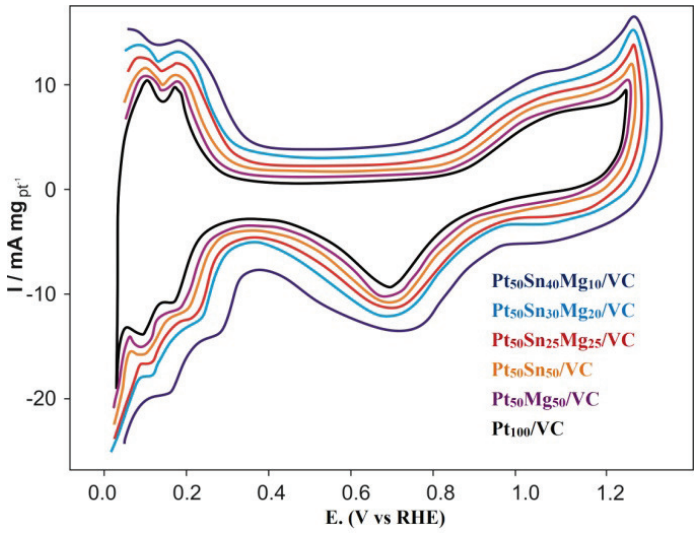

Fig. 4.5-(a) Cyclic voltammogram representations of $Pt_{50}Sn_{40}Mg_{10}$/VC, $Pt_{50}Sn_{30}Mg_{20}$/VC, $Pt_{50}Sn_{25}Mg_{25}$/VC, $Pt_{50}Sn_{50}$/VC, $Pt_{50}Mg_{50}$/VC and Pt_{100}/VC nanoparticles in the absence of fuel.

Table 4.3 Cyclic voltammetry predictions of $Pt_{50}Sn_{40}Mg_{10}$/VC, $Pt_{50}Sn_{30}Mg_{20}$/VC, $Pt_{50}Sn_{25}Mg_{25}$/VC, $Pt_{50}Sn_{50}$/VC, $Pt_{50}Mg_{50}$/VC and Pt_{100}/VC nanoparticles.

Nanoparticles	Scan rate @ 50 mV/s	
	Maximum output voltage (mV *versus* RHE)	Corresponding current density (mA/cm^2)
Pt_{100}/VC	888	4.5
$Pt_{50}Mg_{50}$/VC	876	24.6
$Pt_{50}Sn_{50}$/VC	889	25.8
$Pt_{50}Sn_{25}Mg_{25}$/VC	890	41.6
$Pt_{50}Sn_{30}Mg_{20}$/VC	895	42.8
$Pt_{50}Sn_{40}Mg_{10}$/VC	905	47.8

To emphasize, the initial-commencement-voltage for the electro-oxidation of alcohol on the trimetallic $Pt_{50}Sn_{40}Mg_{10}$/VC, $Pt_{50}Sn_{30}Mg_{20}$/VC, and $Pt_{50}Sn_{25}Mg_{25}$/VC catalysts were much lower than to that of their counterparts $Pt_{50}Sn_{50}$/VC, $Pt_{50}Mg_{50}$/VC and Pt_{100}/VC nanoparticles.

The potential output values were adjusted with a structural planar area of the prepared catalysts. As can be seen from the voltammogram curves, it is figuring out the one decisive peak (*versus* RHE), obtained from the successive browse is related in the direction of alcohol-oxidation as well as the reversal apex obtained from the backward sweep is related toward oxidation of transitional compounds.

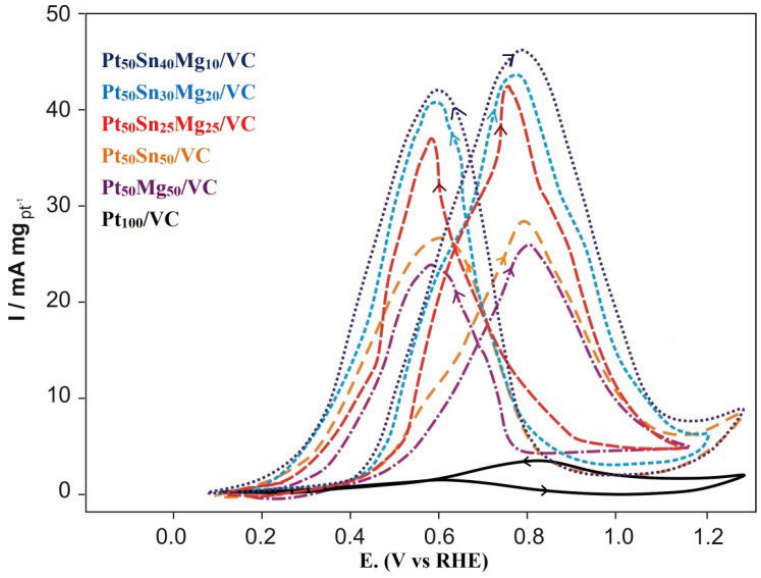

Fig 4.5-(b) Cyclic voltammogram representations of $Pt_{50}Sn_{40}Mg_{10}$/VC, $Pt_{50}Sn_{30}Mg_{20}$/VC, $Pt_{50}Sn_{25}Mg_{25}$/VC, $Pt_{50}Sn_{50}$/VC, $Pt_{50}Mg_{50}$/VC and Pt_{100}/VC nanoparticles in the presence of fuel.

Consequently, the current-density retrieved from $Pt_{50}Sn_{40}Mg_{10}$/VC, $Pt_{50}Sn_{30}Mg_{20}$/VC, $Pt_{50}Sn_{25}Mg_{25}$/VC, $Pt_{50}Sn_{50}$/VC, $Pt_{50}Mg_{50}$/VC and Pt_{100}/VC nanoparticles are 47.8, 42.8, 41.6, 25.8, 24.6 and 4.59 mA/cm^2, respectively, summarizing that trimetallic nanoparticles are approximately double the time greater than that of other catalysts.

Table 4.3 displays the results of cyclic voltammetry in conjunction with the successive-peak output-potentials and the equivalent current-densities related to $Pt_{50}Sn_{40}Mg_{10}$/VC, $Pt_{50}Sn_{30}Mg_{20}$/VC, $Pt_{50}Sn_{25}Mg_{25}$/VC, $Pt_{50}Sn_{50}$/VC, $Pt_{50}Mg_{50}$/VC and Pt_{100}/VC nanoparticles for AOR. Ultimately, it is concluded that pure platinum does not perform well as an efficient catalyst because of its CO adsorption, whereas the incorporation of a second (Sn) and a third metal (Mg) counteract the CO adsorption and enhance the activity of platinum.

4.3.2.2 CA – Chronoamperometry

The term chronoamperometry represents the measurement of currents as a function of time under controlled-potential micro electrolysis. Chronoamperometry is a useful technique in those cases where cyclic voltammetry does not succeed in identifying the electrode mechanisms underlying certain redox mechanisms. With this in mind, the chronoamperometry experiments were carried out for Pt/Sn/Mg nanoparticles supported on VC.

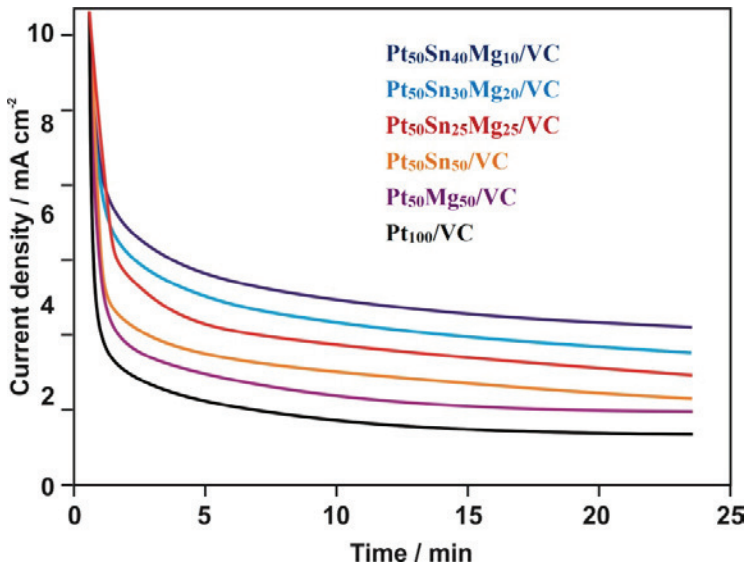

Fig. 4.6 CA of $Pt_{50}Sn_{40}Mg_{10}$/VC, $Pt_{50}Sn_{30}Mg_{20}$/VC, $Pt_{50}Sn_{25}Mg_{25}$/VC, $Pt_{50}Sn_{50}$/VC, $Pt_{50}Mg_{50}$/VC and Pt_{100}/VC nanoparticles.

Fig. 4.6 displays the outcome of stability and long-term operation test conducted at 0.70 V for 25 minutes for the prepared electro-catalysts. It is noted that the initial decrease in current density observed in the first five minutes was due to the attribution of corresponding equilibrium. In the long run, the performance of stability effect on $Pt_{50}Sn_{40}Mg_{10}$/VC nanoparticle is much better than that of the other $Pt_{50}Sn_{30}Mg_{20}$/VC, $Pt_{50}Sn_{25}Mg_{25}$/VC, $Pt_{50}Sn_{50}$/VC, $Pt_{50}Mg_{50}$/VC and Pt_{100}/VC nanoparticles. In addition,

the electrochemical activity towards alcohol oxidation diminishes all together as $Pt_{50}Sn_{40}Mg_{10}$/VC > $Pt_{50}Sn_{30}Mg_{20}$/VC > $Pt_{50}Sn_{25}Mg_{25}$/VC > $Pt_{50}Sn_{50}$/VC > $Pt_{50}Mg_{50}$/VC > Pt_{100}/VC, eventually this approach is identical with the experimental findings of cyclic voltammetry.

4.3.3 Assessment of individual cell performance towards seawater electrolysis

Single cell test is used to investigate the efficiency of the synthesized platinum alloy nanoparticles towards its functional relevance. In the same way, the effect of seawater on $Pt_{50}Sn_{30}Mg_{20}$/VC, $Pt_{50}Sn_{25}Mg_{25}$/VC, $Pt_{50}Sn_{50}$/VC, $Pt_{50}Mg_{50}$/VC and Pt_{100}/VC nanoparticles were studied in a single non-membrane power system for alcohol oxidation. As an illustration, the results of the test are plotted in an origin platform. The **Fig. 4.7** shows a combined plot of potential difference as well as power density versus current density. Though protonated acid has been introduced as an electrolyte, the electrolysis towards alcohol oxidation was poor as compared to seawater. Consequently, this behavior was mainly assigned to the electro generation of seawater towards alcohol oxidation. As shown below, the data of individual cell test performed on various synthesized electrocatalysts have been concluded and tabulated (**Table 4.3**).

Furthermore, it has been observed that the incorporation of the second metal (Sn) and the third metal (Mg) onto Pt on VC support achieved more excellent results in comparison with other catalysts. Maximum power densities obtained for $Pt_{50}Sn_{40}Mg_{10}$/VC, $Pt_{50}Sn_{30}Mg_{20}$/VC, $Pt_{50}Sn_{25}Mg_{25}$/VC, $Pt_{50}Sn_{50}$/VC, $Pt_{50}Mg_{50}$/VC and Pt_{100}/VC are 39.2, 36.7, 30.4, 29.0, 20.4 and 6.7 mW/cm^2, respectively (Table 4.4).

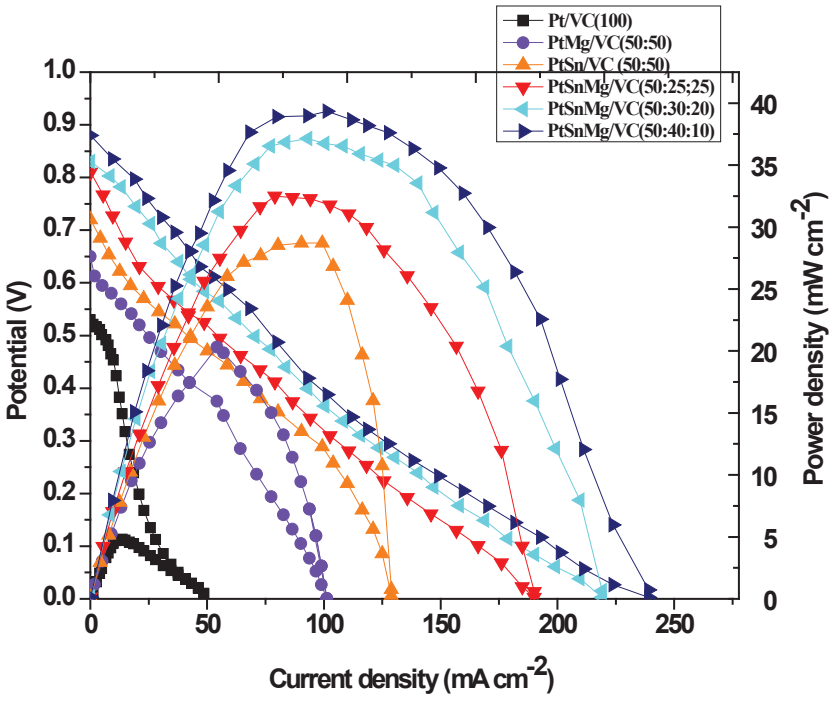

Fig 4.7 Potential difference and power density curves for $Pt_{50}Sn_{40}Mg_{10}$/VC, $Pt_{50}Sn_{30}Mg_{20}$/VC, $Pt_{50}Sn_{25}Mg_{25}$/VC, $Pt_{50}Sn_{50}$/VC, $Pt_{50}Mg_{50}$/VC and Pt_{100}/VC nanoparticles.

Moreover, the analysis of electro generation on seawater power system indicates independently that the presence of a fractional quantity of third metal (Mg) alone be associated with magnesium doped platinized-tin alloy supported on Vulcan carbon nanoparticles intensify the AOR. As a matter of fact, Ribeiro et al, (2007) also discovered comparable observations towards alcohol oxidation in the presence of platinum alloy catalysts prepared by various methods. Obviously, the electro-generation of seawater in non-membrane fuel cell systems suggests that only less amount of third metal helps to amplify the activity of ternary platinum alloy catalysts in alcohol oxidation reactions.

Table 4.4 Analysis of individual cell performance towards seawater electrolysis.

Nanoparticles	Potential (V)	Highest power density (mW/cm^2)	Highest current density (mA/cm^2)
Pt_{100}/VC	**0.53**	**6.7**	**48.7**
$Pt_{50}Mg_{50}$/VC	**0.65**	**20.4**	**100.1**
$Pt_{50}Sn_{50}$/VC	**0.72**	**29.0**	**129.1**
$Pt_{50}Sn_{25}Mg_{25}$/VC	**0.81**	**30.4**	**189.6**
$Pt_{50}Sn_{30}Mg_{20}$/VC	**0.83**	**36.7**	**219.2**
$Pt_{50}Sn_{40}Mg_{10}$/VC	**0.88**	**39.2**	**239.1**

4.4 CONCLUSIONS

In this work, the study of ethanol oxidation in presence of seawater on carbon-supported Pt–Sn–Mg ternary nanoparticles has revealed details concerning the activity and stability of the catalysts in membraneless fuel cells. The maximum activity for ethanol oxidation was found for the $Pt_{50}Sn_{40}Mg_{10}$/VC than the $Pt_{50}Sn_{30}Mg_{20}$/VC, $Pt_{50}Sn_{25}Mg_{25}$/VC, $Pt_{50}Sn_{50}$/VC, $Pt_{50}Mg_{50}$/VC and Pt_{100}/VC. The significantly enhanced catalytic activity for ethanol oxidation can be attributed to the high dispersion of ternary catalysts and to Mg acting as a promoting agent along with the electrogeneration of seawater. XRD results showed the homogenous alloy structure of Pt, Sn and Mg. The TEM images indicated an average size of $Pt_{50}Sn_{40}Mg_{10}$/VC, $Pt_{50}Sn_{30}Mg_{20}$/VC and $Pt_{50}Sn_{25}Mg_{25}$/VC nanoparticles were 2.9-3.2 nm. The atom ratio of Pt, Sn and Mg from EDX analyses was close agreement with the original precursor concentration. The composition of ternary $Pt_{50}Sn_{40}Mg_{10}$/VC nanoparticles can be conveniently controlled

by adjusting the initial metal salt solution and preparation conditions. The electrochemical experiments showed that the $Pt_{50}Sn_{40}Mg_{10}$/VC nanoparticles have higher catalytic activity than that of the other catalysts in sea water electrolyte. It is also oberved that the activity of electrocatalysts were diminished in the absence of seawater. We expect that the MLEFC may be a promising candidate for practical fuel cells to establish a clean and sustainable future energy. Further work is necessary to characterize the catalysts using different surface analysis techniques and to conduct tests of these electrocatalysts in microfluidic membraneless fuel cells in presence and absence of seawater.

REFERENCES

1) **Arun A, Gowdhamamoorthi M, Kiruthika S, Muthukumaran B, 2014,** 'Electrochemical characterization of Pt-Ru-Ni/C anode electrocatalyst for methanol electrooxidation in membraneless fuel cells', *J. Electrochem. Soc,* Vol. 161, p. F311.

2) **Beyhan S, Leger JM, Kadirgan F, 2013,** 'Pronounced synergetic effect of the nano sized PtSnNi/C catalyst for ethanol oxidation in direct ethanol fuel cell', *Appl. Catal. B Environ*. Vol.130, p.305–313.

3) **Bonesi AR, Moreno MS, Triaca WE, Luna AMC, 2010,** 'Modified catalytic materials for ethanol oxidation', *Int. J. Hydrogen Energy*, Vol.35, p.5999–6004.

4) **Cao J, Du C, Wang SC, Mercier P, Zhang X, Yang H, 2007,** 'The production of a high loading of almost monodispersed Pt nanoparticles on single walled carbon nanotubes for methanol oxidation', *Electrochem. Commun*. Vol.9, p.735–740.

5) **Chen W, Wei X, Zhang Y, 2014,** 'A comparative study of tungsten modified PtRu electrocatalysts for methanol oxidation', *Int. J. Hydrogen Energy*. Vol.39, p.6995–7003.

6) **Choban ER, Markoski LJ, Wieckowski A, Kenis PJA, 2004,** 'Microfluidic fuel cell based on laminar flow', *J. Power Sources*, Vol. 128, p.54.

7) **Choi WC, Woo SI, 2003,** 'Bimetallic Pt-Ru nanowire network for anode material in a direct-methanol fuel cell', *J. Power Sources*. Vol.124, p.420–425.

8) **Choi JH, Park KW, Park IS, Nam WH, Sung YE, 2004,** 'Methanol electro-oxidation and direct methanol fuel cell using Pt/Rh and Pt/Ru/Rh alloy catalysts', *Electrochimica Acta*., Vol.50, p.787.

9) **Colmati F, Antolini E, Gonzalez ER, 2007,** 'Ethanol oxidation on a carbon – supported $Pt_{75}Sn_{25}$ electrocatalyst prepared by reduction with formic acid: Effect of thermal treatment', *Appl. Catal. B*, Vol.73, p.106.

10) **Cotton FA, Wilkinson G, 1998,** Wiley Interscience, New York, p. 812.

11) **Gasteiger HA, Markovic N, Ross PN, Cairns EJ, 1993,** 'CO electrooxidation on well characterized Pt – Ru alloys', *J. Phys. Chem*., Vol.97, p.12020–12029.

12) **Gowdhamamoorthi M, Arun A, Kiruthika S, Muthukumaran B, 2014,** 'Perborate as novel fuel for enhanced performance of membraneless fuel cells', *Ionics*. Vol.20, p.1723–1728.

13) **Jayashree RS, Yoon SK, Brushett FR, Lopez Montesinos PO, Natarajan D, Markoski LJ, Kenis PJA, 2010,** 'On the performance of membraneless laminar flow-based fuel cells', *Journal of Power Sources*, Vol.195, p.3569.

14) **Kang DK, Noh CS, Park ST, Sohn JM, Kim SK, Park YK, 2010,** 'The effect of PtRuW ternary electrocatalysts on methanol oxidation reaction in direct methanol fuel cells', *Korean J. Chem. Eng*. Vol.27 p.802–806.

15) **Luo J, Njoki PN, Lin Y, Mott D, Wang L, Zhong CJ, 2006,** 'Characterization of carbon supported AuPt nanoparticles for electrocatalytic methanol oxidation reaction', *Langmuir*., Vol.22, p.2892.

16) **Markovic NM, Gasteiger HA, Ross PN, Jiang XD, Villegas I, Weaver MJ, 1995,** 'Electrooxidation mechanisms of methanol and formic-acid on Pt Ru alloy surfaces', *Electrochimica Acta*, Vol.40, p.91.

17) **Neto AO, Dias RR, Tusi MM, Linardi M, Spinace EV, 2007,** 'Electro-oxidation of methanol and ethanol using PtRu/C, PtSn/C and PtSnRu/C electrocatalysts prepared by an alcohol-reduction process', *J. Power Sources*. Vol.166, p.87–91.

18) **Ponmani K, Durga S, Arun A, Kiruthika S, Muthukumaran B, 2014,**

'Development of membraneless sodium perborate fuel cell for media flexible power generation', *International Journal of Electrochemistry*, Vol.2014, p.1–9.

19) **Radmilovic V, Gasteiger HA, Ross PN, 1995,** 'Structure and chemical composition of a supported Pt–Ru electrocatalysis for methanol oxidation', *J. Catal*. Vol.154, p.98–106.

20) **Ren XM, Zelenay S, Thomas S, Davey J, Gotttesfeld S, 2000.** 'Recent advances in direct methanol fuel cells at Los Alamos National Laboratory', *J. Power Sources*, Vol.86, p.111.

21) **Shobha T, Aravinda CL, Bera P, Devi LG, Mayanna SM, 2003,** 'Characterization of Ni–Pd alloy as anode for methanol oxidative fuel cell', *Mater. Chem. Phys*., Vol.80, p.656.

22) **Sivakumar P, Tricoli V, 2006,** 'Pt-Ru-Ir nanoparticles prepared by vapor deposition as a very efficient anode catalyst for methanol fuel cells', *Electrochem. Solid-State Lett*., Vol.9, p.A167.

23) **Vigier F, Coutanceau C, Hahn F, Belgsir EM, Lamy C, 2004,** 'On the mechanism of ethanol electrooxidation on Pt and PtSn catalysts: electrochemical and in situ IR reflectance spectroscopy studies', *J. Electroanal. Chem*. Vol.563, p.81–89.

24) **Wang ZB, Zuo PJ, Yin GP, 2009,** 'Effect of W on activity of Pt-Ru/C catalyst for methanol electrooxidation in acidic medium', *J. Alloys Compd*, Vol.479, p.395-400.

25) **Wang Z, Zuo P, Wang G, Wang J, Yin G, 2009,** 'Effect of annealing heat treatment on stability of Pt-Ru-Ni/C catalyst for direct methanol fuel cell', *Chinese J. Power Sources*, Vol.1, p.7.

26) **Xu J, Hua K, Sun G, Wang C, Lv X, Wang Y, 2006,** 'Electrooxidation of methanol on carbon nanotubes supported Pt–Fe alloy electrode', *Electrochem. Commun*., Vol.8, p.982.

27) **Yajima T, Uchida H, Watanabe M, 2004,** 'In-situ ATR-FTIR spectroscopic study of electro oxidation of methanol and adsorbed CO at Pt-Ru alloy', *J. Phys. Chem. B*. Vol.108, p.2654–2659.

28) **Yamaguchi T, Kuroki H, Miyata, 2005,** 'DMFC performances using a porefilling polymer electrolyte membrane for portable usage', *Electrochem. Commun*., Vol.7, p.730.

29) **Zhou Z, Wang S, Zhou W, Wang G, Jiang L, Li W, 2003,** 'Novel synthesis of highly active Pt/C cathode electrocatalyst for direct methanol fuel cell', *Chem. Commun*. p.394–395.